A hydrogen-dependent geochemical analogue of primordial carbon and energy metabolism

Martina Preiner, Kensuke Igarashi, Kamila Muchowska, Mingquan Yu, Sreejith J. Varma, Karl Kleinermanns, Masaru K. Nobu, Yoichi Kamagata, Harun Tüysüz, Joseph Moran, et al.

A hydrogen dependent geochemical analogue of primordial carbon and energy metabolism

Martina Preiner[1,8], Kensuke Igarashi[2,8], Kamila B. Muchowska[3,8], Mingquan Yu[4,8], Sreejith J. Varma[5], Karl Kleinermanns[6], Masaru K. Nobu[7], Yoichi Kamagata[7], Harun Tüysüz[4]*, Joseph Moran[3]*, William F. Martin[1]*

[8] These authors contributed equally: Martina Preiner, Kensuke Igarashi, Kamila B. Muchowska, Mingquan Yu

* e-mail: bill@hhu.de; moran@unistra.fr; tueysuez@kofo.mpg.de

[1] Institute of Molecular Evolution, University of Düsseldorf, 40225 Düsseldorf, Germany

[2] Bioproduction Research Institute, National Institute of Advanced Industrial Science and Technology (AIST), 2-17-2-1 Tsukisamu-Higashi, Toyohira-ku, Sapporo, Hokkaido 062-8517, Japan

[3] Université de Strasbourg, CNRS, ISIS UMR 7006, F-67000 Strasbourg, France

[4] Max-Planck-Institut für Kohlenforschung, Kaiser-Wilhelm-Platz 1, 45470 Mülheim an der Ruhr, Germany

[5] Charité – Universitätsmedizin Berlin, Laboratory "Biochemistry and System Biology of the Metabolism", Charitéplatz 1, 10117 Berlin, Germany

[6] Institute for Physical Chemistry, University of Düsseldorf, 40225 Düsseldorf, Germany

[7] Bioproduction Research Institute, National Institute of Advanced Industrial Science and Technology (AIST), 1-1-1 Higashi, Tsukuba, Ibaraki 305-8566, Japan

Keywords: Origin of life, serpentinization, hydrothermal vents, early Earth, abiotic carbon fixation, protometabolism, geochemical catalysis.

Editorial Summary

Three iron minerals found in alkaline hydrothermal vents are shown to convert CO_2 and H_2 into formate, acetate and pyruvate in water, suggesting that such reactions could have paved the way for early metabolism.

Abstract

Hydrogen gas, H_2, is generated by alkaline hydrothermal vents through an ancient geochemical process called serpentinization in which water reacts with iron containing minerals deep within the Earth's crust. H_2 is the electron donor for the most ancient and the only energy releasing route of biological CO_2 fixation, the acetyl-CoA pathway. At the origin of metabolism, CO_2 fixation by hydrothermal H_2 within serpentinizing systems could have preceded and patterned biotic pathways. Here we show that three hydrothermal minerals—greigite (Fe_3S_4), magnetite (Fe_3O_4) and awaruite (Ni_3Fe)—catalyse the fixation of CO_2 with H_2 at 100°C under alkaline aqueous conditions. The product spectrum includes formate (up to 200 mM), acetate (up to 100 μM), pyruvate (up to 10 μM), methanol (up to 100 μM), and methane. The results shed light on both the geochemical origin of microbial metabolism and on the nature of abiotic formate and methane synthesis in modern hydrothermal vents.

Organic synthesis in hydrothermal vents is relevant to life's origin because the reactions involve sustained energy release founded in the disequilibrium between CO_2 and the vast amounts of molecular hydrogen, H_2, generated in the Earth's crust during serpentinization[1–9]. Hydrogen has been a source of electrons and energy since there was liquid water on the early Earth and it fuelled early anaerobic ecosystems in the Earth's crust[1,8,10]. In biochemistry, the acetyl-CoA pathway of CO_2 fixation uses the electrons and energy of H_2 to simultaneously supply three key requirements for life: reduced carbon in the form of acetyl groups, electrons in the form of reduced ferredoxin, and ion gradients for energy conservation in the form of ATP[11,12]. The pathway is linear, not cyclic, it releases energy rather than requiring energy input and its enzymes are replete with primordial metal cofactors[13,14]. It traces to the last universal common ancestor[15] and abiotic, geochemical organic syntheses resembling segments of the pathway occur in hydrothermal modern vents[2,3]. Laboratory simulations of the acetyl-CoA pathway's reactions include the nonenzymatic synthesis of thioesters from CO and methylsulfide[16], the synthesis of acetate[17] and pyruvate[18] from CO_2 using native iron or external electrochemical

potentials[19] as the electron source. Enzymatic versions of those abiotic reactions occur in core energy metabolism of acetogens and methanogens[11–14], ancient anaerobic autotrophs that live from H_2 and CO_2 via the acetyl-CoA pathway and that still inhabit the crust today[14]. Though the enzymes that catalyse the modern microbial reactions are well investigated[11–14], the catalysts promoting the abiotic reactions in vents today, and that might have been instrumental at life's origin, are poorly understood[2]. A fully abiotic analogue of the acetyl-CoA pathway from H_2 and CO_2 as it occurs in life has not been reported to date.

To probe the mechanisms of hydrothermal metabolic reactions emulating ancient pathways, we investigated three different iron minerals that naturally occur in hydrothermal systems: greigite (Fe_3S_4), magnetite (Fe_3O_4), and the nickel iron alloy awaruite (Ni_3Fe). Magnetite (Fe_3O_4) and awaruite (Ni_3Fe) are common constituents of serpentinizing systems[20] and are more stable under alkaline conditions than greigite[21,22]. Fe_3O_4, like H_2, is a main end product of serpentinization, it is formed from water dependent oxidation of iron(II) silicates[23]. In chemical industry, iron based materials are the catalysts of choice for diverse industrial processes including Haber-Bosch (fixation of N_2) and Fischer-Tropsch syngas (CO and H_2) conversion to hydrocarbons[7]. Ni_3Fe is an intermetallic compound that forms in serpentinizing systems at high H_2 partial pressures and very low H_2S fugacities[5,20], via the reduction of iron(II) and nickel(II) compounds. It is common in Ni-containing serpentinizing systems, where it is usually deposited as small grains[20]. Fe_3S_4 is formed under conditions of high H_2S activity[5,21], as a transient intermediate in the conversion of mackinawite to pyrite[22,24]; it shares structural similarity with the iron sulfur clusters of many modern enzymes[6]. Iron sulfides can be found at the surface of hydrothermal vents as small compartments[21] or as nanoparticles in hydrothermal plumes[25] as well as in meteorites[26]. Iron minerals have long been regarded as ancient catalysts[6,16,27] although the key initial reaction connecting the inorganic and the organic world—CO_2 fixation with H_2 as the reductant—has not been reported using iron mineral catalysts under biologically relevant conditions[19].

Results

Although very different in structure and composition (Fig. 1), greigite, magnetite and awaruite are geochemically synthesised in hydrothermal systems from pre-existing divalent iron and nickel minerals during serpentinization[5,8,28]. X-ray diffraction (XRD) applied to our laboratory preparations of colloidal Fe_3S_4 and Ni_3Fe nanoparticles (for details of synthesis, see Methods) as well as commercial Fe_3O_4 reveals their characteristic patterns of crystal structures (Fig. 1).

Building on evidence for catalytic reactivity in previous reports[16–19], we investigated the ability of greigite, magnetite and awaruite to promote the reduction of CO_2 with H_2 in water. Under very mild hydrothermal conditions—at 100 °C under 2 bar H_2/CO_2 (80:20)—formate and acetate synthesis from H_2 and CO_2 occurs readily in nearly neutral and alkaline aqueous solution in the presence of Fe_3S_4 (Fig. 2a). While only formate was detected at 20 °C, formate and acetate were found at 60 °C, which is close to the temperature of vent effluent (ca. 70°C) in the Lost City hydrothermal field (Fig. 2b)[29]. At 100 bar, Fe_3S_4 catalyses the synthesis of formate and methane from H_2 and CO_2 (Fig. 2c), but not from CO (Extended Data Fig. 4b). Here, methane and formate production is almost stoichiometric relative to hydrogen decrease. For 14 mM H_2 consumed, 1 mM of formate (1 H_2 per molecule of formate) and 2.3 mM of methane (4 H_2 per molecule of methane) are produced, leaving only 3.8 mM of H_2 that might go into acetate synthesis (which was below detection in this experimental setup). At 2 bar, formate accumulates to over 2 mM within 4 h, while acetate requires between 4 and 8 h to become detectable (Fig. 2d). Notably, formate and methane are the main products of abiotic organic synthesis observed in the effluent of modern serpentinizing hydrothermal systems[9,30–33].

We found that magnetite, like greigite, catalyses the aqueous synthesis of formate and acetate in the range of 10 μM to 1 mM from H_2 and CO_2, but also the formation of methanol and pyruvate under mild (25 bar H_2/CO_2, 40:60 ratio and 100 °C) hydrothermal conditions (Fig. 3a). Pyruvate is a crucial intermediate of carbon and energy metabolism in all microbes and the main product of CO_2 fixation in autotrophs that use the acetyl-CoA pathway[11]. It accumulates at 5–10 μM in the presence of Fe_3O_4 across the pH range of 6–10, when either native iron (Fe) or H_2 is used as the reductant (Fig. 3a). Fe_3O_4 generates a generally uniform product distribution across conditions tested, also when smaller amounts of catalyst are used (Extended Data Fig. 6b). Additionally, we investigated different amounts of Fe as a reductant, showing that its

impact on product concentrations is low even if a large excess of Fe was used. Both Fe and Fe_3O_4 formed a solid disc after the reaction, which probably hindered further oxidation of Fe and thus further accumulation of reduced carbon compounds (Extended Data Fig. 7a).

At 100 °C, awaruite catalyses the synthesis of acetate and methanol in the 10–100 µM range at pH 5–8 whereby either the native alloy itself, H_2, or native Fe can function as the reductant, albeit with differing efficiency and product distribution (Fig. 3b). At alkaline conditions, with either native Fe or H_2 as reductant, formate accumulates in the 200 mM range with 1 mmol metal atoms as catalyst. Physical contact between awaruite and native iron is not required for product formation (Extended Data Fig. 7b). In the case of awaruite, lower temperatures improved pyruvate synthesis (Fig. 4a), similar to previous studies[18]. Pyruvate is formed under alkaline conditions at 70 °C (Fig. 4a), even at lower catalyst amounts than previously used (0.5 mmol metal atoms), and reaches 10 µM when higher amounts of catalyst are used (Fig. 4b). This suggests that pyruvate production in reactions with smaller amounts of awaruite likely occurs, but is below the detection limit of the ^{1}H-NMR spectroscopy used here. Using even less Ni_3Fe (0.05 mmol metal atoms) is still effective for formate, acetate and methanol formation in thermal gradients from 100 °C to 30 °C (Extended Data Fig. 6a and c), conditions similar to those of natural alkaline hydrothermal vents[34]. Catalysts are required for the reaction, controls without catalysts yielded only trace levels of product (Extended Data Fig. 2b and c and Supplementary Tabs. 6 and 7).

In some experiments using Ni_3Fe, we detected ethanol in concentrations up to over 100 µM (Extended Data Fig. 5b). We observed trace amounts of methane (ca. 19 ppm) in awaruite catalysed reactions (Extended Data Fig. 8), which is substantially less than detected in an earlier report using H_2 and CO_2 for 1–2 weeks at 500 bar and 200–400 °C with awaruite as the catalyst[35]. The hydrothermal conditions we found for the synthesis of organics from H_2 and CO_2 over 16 hours with awaruite as catalyst are mild enough in terms of temperature and energetics to permit microbial growth. Of the catalysts employed, only awaruite showed minor alteration after reaction, probably due to mild oxidation (Fig. 1g–i). Formate accumulation catalysed by awaruite reflects the near-equilibrium interconversion of H_2-CO_2 and formate[36].

To avoid contamination, no organic buffers were employed in any of our experiments. Because Fe_3S_4 is sensitive to high pH, phosphate buffer was employed when greigite was the catalyst.

In the experiments with magnetite and awaruite, no buffers were used. In Figs. 3 and 4, blue bars indicate reactions where the starting pH was ~11 through addition of KOH to generate alkaline vent conditions; the pH measured at completion depends on the amount of utilised mineral and metal in addition to the amount of CO_2 dissolved and organic acid synthesised. No water loss, which would potentially distort the product concentrations, was detected in any of our experiments.

Sustained synthesis of reactive organic compounds was essential at the origin of metabolism and had to be thermodynamically favourable. Equations **1–5** show the redox reactions taking place between CO_2 and H_2 to form formate (**1**), methanol (**2**), acetate (**3**), pyruvate (**4**), and methane (**5**).

$$H_2 + CO_2 \rightarrow HCOO^- + H^+ \quad \textbf{1}$$

$$3\ H_2 + CO_2 \rightarrow CH_3OH + H_2O \quad \textbf{2}$$

$$4\ H_2 + 2\ CO_2 \rightarrow CH_3COO^- + 2H_2O + H^+ \quad \textbf{3}$$

$$5\ H_2 + 3\ CO_2 \rightarrow CH_3(CO)COO^- + 3\ H_2O + H^+ \quad \textbf{4}$$

$$4\ H_2 + CO_2 \rightarrow CH_4 + 2\ H_2O \quad \textbf{5}$$

The changes in Gibbs free energy, ΔG, for six of the H_2-dependent reactions reported here are given in Table 1 (detailed datasets are shown in Supplementary Tabs. 2 and 3). The synthesis of observed products is close to equilibrium or exergonic. For most compounds and conditions, product generation did not reach equilibrium, indicating kinetic inhibition of the reactions. Only H_2-dependent reduction of CO_2 to formate approached equilibrium in the presence of greigite or awaruite (according experiments in Fig. 2a and 3b). Pyruvate and CH_4 production were only detected under specific conditions despite being exergonic in nearly all treatments. For example, in treatments with H_2 and magnetite, pyruvate generation was only detected under alkaline conditions (Fig. 3a), while in treatments with H_2 and awaruite, pyruvate generation was only detected under alkaline conditions and when the amount of mineral was increased (Fig. 4a). H_2-dependent reduction of formate to acetate (eq. **3** – eq. **1**; $3H_2 + CHOO^- + CO_2 \rightarrow CH_3COO^- + 2\ H_2O$) consistently reached similar ΔG values for each mineral regardless of pH and mineral amount (roughly –72 kJ mol^{-1} for greigite, –89 kJ mol^{-1} for magnetite, and –115

kJ mol^{-1} for awaruite at 100 °C), suggesting the possibility of shared features between the minerals' catalytic mechanisms. None of the three minerals catalyses acetate synthesis to completion ($\Delta G << 0$), suggesting the possible presence of kinetic barriers and an opportunity for energetic coupling. For those reactions in which no H_2 was added, only native metals were available as reductant (Extended Data Figs. 3, 5a and 7), likely generating intermediate H_2 from water.

Discussion

When greigite, magnetite or awaruite are used as catalysts, the synthesis of formate, acetate, methanol and pyruvate from H_2 and CO_2 under hydrothermal conditions is facile. The synthesis of formate and acetate is furthermore robust to the catalyst employed. The main product we observed is formate (Figs. 2–4), which is also the main organic product of abiotic organic synthesis found in alkaline hydrothermal vent effluent[9,31,37,38]. We propose a mechanism for the catalysed two-electron reduction of CO_2 to formate for all three minerals (Extended Data Fig. 10).

Formate synthesis from H_2 and CO_2 was anticipated by earlier studies[39,40], and formate synthesis from CO_2 has been reported at high temperatures (>250 °C) and pressures (>300 bar) with hydrothermal minerals[41]. But the amounts of formate that we observe with Ni_3Fe at moderate temperature and pressure (70°C to 100 °C in 25 bar H_2/CO_2 atmosphere), as well as the accumulation of acetate and pyruvate reveal an unexpected correspondence between the spontaneous H_2-dependent CO_2 reduction and metabolism. We see a clear tendency of Ni containing compounds to preferentially produce formate in high concentrations[18], while pyruvate accumulation is preferentially observed with Fe. These product-catalyst specificities are reflected in the active site metals of the corresponding enzymes of the modern acetyl-CoA pathway[11–13,42–47].

Under physiological conditions, the reducing power of H_2 is insufficient to reduce CO_2. Microbes studied so far reduce CO_2 with electrons from H_2 employing flavin-based electron bifurcation to synthesise reduced iron sulfur clusters in ferredoxin for CO_2 fixation[12,48]. This biological CO_2 fixation usually also entails ion gradients[48,49]. The reactions reported here require neither electron bifurcation nor ion gradients. With suitable inorganic catalysts that activate both H_2 and CO_2 to enable their reaction, products of the acetyl-CoA pathway (Fig. 2, 3 and 4) are formed without the addition of organic cofactors.

With the exception of ethanol, the reaction products we observe correspond exactly to those of the biological acetyl-CoA pathway to pyruvate[11] (Fig. 5). No other reaction products were observed. That is, the mineral catalysed H_2-dependent reduction of CO_2 delivers a very discrete subset of the possible chemical structures: one that constructs the backbone of carbon and

energy metabolism in primitive anaerobic autotrophs[11–15]. The acetyl-CoA pathway[11,14] entails eleven main enzymes totalling ~15,000 amino acid residues[13,42–46] plus six organic cofactors each with its own complex biosynthesis[14]. The bacterial and archaeal versions of the pathway involve evolutionarily unrelated enzymes but chemically similar methyl synthesis routes[6,11,14]. The reactions of the acetyl-CoA pathway employed by modern metabolism (Fig. 5) involve the stepwise conservation of chemical energy during CO_2 fixation as acetyl-nickel, acetyl-thioester, acetyl-phosphate, and ATP synthesis via substrate level phosphorylation (marked with an asterisk in Fig. 5)[11–14]. Although the nature of the catalyst bound intermediates of the biological pathway from H_2 and CO_2 to methane, acetate and pyruvate is known[11–14], the identity of the catalyst-bound intermediates of the mineral catalysed reactions is not.

Proposals for the nature of primordial CO_2 fixation and energy conservation at biochemical origins typically posit the participation of external energy sources[50] such as UV light[51], heat, impact, pressure, electrical currents, or ion gradients[28] to push organic synthesis forward. The reactions reported here require no additional energy source for a protometabolic acetyl-CoA pathway to unfold from H_2 and CO_2 other than the natural reactivity of two gasses and metal catalysts, indicating that neither membranes, though essential for the emergence of free-living cells[6,52–54], nor external potentials[19,55] were required for primordial CO_2 fixation along an exergonic, H_2-dependent, nonenzymatic pathway to C3 products. The energy for the synthesis of compounds capable of phosphorylating ADP via substrate level phosphorylation[6,11,12]—for reactions reported here, and for those of the enzymatically catalysed acetyl-CoA pathway—stems from the exergonic synthesis of biologically relevant organic compounds from H_2 and CO_2. Our findings suggest that abiotic, geochemical versions of the energy releasing reactions underlying the acetyl-CoA pathway very likely preceded the enzymes that catalyse it today[11,14,18,56]. The simplicity and primordial nature of these reactions furthermore suggests that metabolism elsewhere could initiate by a similar route.

Methods

General information. An overview of the performed experiments can be found in Extended Data Fig. 1, and relevant controls – in Extended Data Figs. 2 and 3 and Supplementary Tabs. 4–7. The quantity of each transition metal reagent tested as carbon fixation catalyst was normalised to contain the same number of mmol of metal atoms across the experiments. For example, "1 mmol metal atoms" corresponds to: 0.33 mmol greigite Fe_3S_4 (99 mg), 0.33 mmol magnetite Fe_3O_4 (77 mg), and 0.25 mmol awaruite Ni_3Fe (58 mg). Each reaction was performed in at least triplicate. Information on suppliers, grade and purity of all used reagents are listed in the Supplementary Information.

Synthesis of greigite (Fe_3S_4). Every piece of apparatus used in greigite synthesis was stored in an anaerobic chamber (Coy Laboratory Products) under a gas mixture of $N_2/H_2/CO_2$ (80:5:15) for at least 48 h before use, to remove the residual oxygen. Reagents for greigite synthesis were purged with N_2 before use unless otherwise stated. Amorphous FeO(OH) was synthesised as reported previously[57] and suspended in Milli-Q water (0.30 mol/L) under air atmosphere. After purging with N_2, this suspension was stored in a glass bottle under $N_2/H_2/CO_2$ (80:5:15). The solutions of Na_2S (1.0 M) and H_2SO_4 (2.0 M) were prepared as reported previously[58] and stored in a glass bottle under N_2. Greigite was synthesised in a solid-gas reaction system as reported previously[58] with slight modifications. In brief, amorphous FeO(OH) (0.66 mmol, 2.2 mL of water suspension) was aliquoted to a glass reaction vessel, and a test tube containing 1.0 mL of the Na_2S solution was placed in the vessel inside the anaerobic chamber. The vessel was sealed with an ETFE-coated butyl rubber stopper and an aluminium seal. Then, the vessel was removed from the anaerobic chamber and the headspace gas was replaced with Ar. After returning the vessel into the anaerobic chamber, H_2S gas was generated inside the vessel by injecting 0.5 mL of the H_2SO_4 solution to the Na_2S solution in the test tube using a disposable Myjector syringe (Terumo). The vessel was incubated at 80 °C for 3 hours. The resulting greigite suspension was collected by pipetting from several reaction vessels, washed with 0.5 M HCl and then rinsed with N_2-purged Milli-Q water in the anaerobic chamber as described previously[58].

CO_2 fixation catalysed by greigite. Synthesised greigite (0.33 mmol) was resuspended in 3 mL of potassium phosphate buffer (20 mM) of a designated pH. The greigite suspension was placed

in a fresh glass reaction vessel, which was then sealed with an ETFE-coated butyl rubber stopper and an aluminium seal. The vessel was then removed from the chamber, and the headspace gas was replaced with H_2/CO_2 (80:20) or CO_2 outside the chamber. The vessels were incubated at 100 °C over 4 to 24 h.

HPLC analysis (greigite experiments). Liquid phase components were analysed on a D-2000 LaChrom Elite HPLC system (Hitachi), equipped with Aminex® HPX-87H column (300 mm, 7.8 mm I.D.; Bio-Rad Laboratories) and an L-2400 UV detector at 240 nm and L-2490 RI detector as described previously[59]. Supernatants obtained in the CO_2 reduction experiments were collected after centrifugation inside the anaerobic chamber. 10 µL of the obtained supernatants were directly injected into the HPLC circuit and chromatographed under an isocratic flow of 0.7 mL/min (Eluent: 10 mM H_2SO_4 in H_2O). The column temperature was maintained at 50 °C. Identities of the detected analytes were determined by the LC-MS system: Agilent 1200 HPLC (Agilent Technologies) coupled to an HCT Ultra mass spectrometer (Bruker Daltonics), using a Shodex® HILICpak VG-50 2D column (150 mm, 2 mm I.D.; Showa denko). The supernatant prepared as above was mixed with an equal amount of the eluent. Then, 5 µL of the mixture was injected into the HPLC circuit and chromatographed under an isocratic flow of 0.1 mL/min (Eluent: a mixture of acetonitrile and 0.25% ammonia water with 80:20 ratio). Column temperature was maintained at 30 °C.

High-pressure measurements (greigite experiments). A previously developed[60] high-pressure incubation system was utilised for the high-pressure CO_2 (Fig. 2c) and CO (Extended Data Fig. 4b) reduction reactions in this study. The system consisted of an incubation vessel (stainless steel with Sulfinert® coating on its internal wall, volume 150 cm^3; Swagelok), inflow/outflow tubes with valves (Swagelok), and a 500D automated syringe pump (Teledyne Isco). The greigite suspension was placed in the reaction vessel inside the anaerobic chamber. After sealing the vessel with inflow and outflow tubes, the headspace gas was replaced with H_2+CO_2 (80:20) through a rubber septum equipped with an inflow tube, via a needle. This vessel was then connected to the syringe pump via the inflow tube to complete the incubation system. Potassium phosphate buffer was injected by the syringe pump to reach a hydrostatic pressure of 100 bar. Incubation at 60°C started after H_2 and CO_2 were completely dissolved in the liquid phase (verified by GC analysis). Samples were periodically collected via the outflow tube while keeping the same hydrostatic pressure through automated pressure control of the syringe pump.

Gas analysis (greigite experiments). Gas phase measurements were carried out on a gas chromatograph GC-2014 (Shimadzu) as described previously[59]. Depending on the target gas component, different columns and detectors were used: a Rt-QPLOT (30 m, 0.32 mm I.D, 10 μm F.T.; Restek) with flame ionization detector (FID) for CH_4, molecular sieve 13X column (2 m, 3 mm I.D.; Shimadzu) with a thermal conductivity detector (TCD) for H_2 and CO, and activated charcoal column (2.0 m, 3 mm, 60/80 mesh; Shinwa Chemical Industries) with TCD for CO_2. Pure He and Ar were used as carrier gases for FID and TCD, respectively. The gasses were identified by GC-mass spectrometry (GC-MS) using two systems: 1) TQ8040 NX GC-MS (Shimadzu) equipped with a polar capillary column (TC-70, 30 m, 0.25 mm I.D., 0.25 μm F.T.; GL Sciences); 2) QP2010 Plus GC-MS (Shimadzu) equipped with Rt-Q-BOND (15 m, 0.32 mm I.D., 10 μm F.T.; Restek). Carrier gas in both systems was pure He.

Synthesis of awaruite (Ni_3Fe) nanoparticles. As previously reported[61,62], spent tea leaves can be used as sustainable hard template to synthesise native metal nanoparticles in the desired composition. For the synthesis of nanoparticular Ni_3Fe, washed and dried tea leaves were added into an aqueous solution of $Ni(NO_3)_2 \cdot 6H_2O$ and $Fe(NO_3)_3 \cdot 9H_2O$ (molar ratio of 3:1) and stirred at room temperature for 2 h. The mass ratio of tea leaves and metal precursors was set at 2:1. Due to the low decomposition temperature of the metal nitrate salt (below 200°C), metal oxide nanoparticles can be formed in the pore confinement of the template before its structural damage/combustion. The carbon-based tea leaf template was burned out in air atmosphere (at 550 °C for 4 h) and the resulting Ni_3Fe oxide was washed with 0.1 M HCl solution for 2 h and cleaned with deionised water. Finally, the product was treated in a reductive 10% H_2/Ar flow (100 mL/min) at 500 °C for 2 h to generate the intermetallic Ni_3Fe compound.

CO_2 fixation catalysed by magnetite (Fe_3O_4) and awaruite (Ni_3Fe). Awaruite and magnetite powder (commercial) were placed in a 1.5 mL glass vial. In the case of magnetite experiments and the awaruite experiments displayed in Fig. 2d, a clean PTFE-coated stir bar was added to the vial. All further awaruite experiments were conducted without stir bars. Then, the reaction vials were filled with 1.0 mL of Milli-Q water. Whenever the effect of an increased pH of the reaction mixtures was tested, solid KOH was added into the Milli-Q water before the reaction (45 mg/mL). KOH had been tested for contaminants via the ^{1}H-NMR analysis (Extended Data Fig. 9a). To prevent cross-contamination while allowing for the gas to easily reach the reaction mixture, the vials were closed with caps with punctured PTFE septa. The reaction vials (3–12)

were placed in a stainless-steel pressure reactor (Berghof or Parr) which was then sealed, flushed three times with ca. 5 bar CO_2, pressurised to a final value of 25 bar CO_2 (unless noted otherwise), and heated at the desired temperature (an external heating mantle was used) for 16 h. At a reaction temperature of 100 °C, a maximum pressure of ca. 30 bar was reached. After the reaction, the reactor was allowed to cool down to room temperature (3–4 h from 100 °C, 2–3 h from 70 °C) before sample analysis[18,56].

Experiments with iron powder or hydrogen gas. The experiments were performed according to the general procedure described above, except that 10 mmol (560 mg) Fe^0 powder was first placed in the reaction vials, followed by the mineral tested and no stir bars were added. Further experiments exploring the impact of the amount of Fe^0 powder are displayed in Extended Data Fig. 7a). Whenever H_2 was used in the experiments, the pressure reactor was first flushed with CO_2, then pressurised with 10 bar of H_2 and then brought to 25 bar by adding CO_2 again (H_2/CO_2 approximately 40:60).

Work-up procedure for reaction mixtures (Ni_3Fe and Fe_3O_4). The pH of individual reaction mixtures was determined via TRITEST L pH 1–11 pH papers (Macherey-Nagel) directly after the reaction. The values of the Ni_3Fe experiments were confirmed with a pH-Meter (Lab 875, SI Analytics) and a pH combination microelectrode (A 157 IDS, SI Analytics). The CO_2 dissolved in the reaction mixture during the reaction decreased the reaction pH values due to the formation of carbonic acid. Reaction mixtures that did not contain KOH were either treated with ca. 45 mg solid KOH per 1 mL reaction mixture to precipitate the metal ions as hydroxides (in the case of Fe_3O_4 and Ni_3Fe experiments displayed in Fig. 3), or left untreated (in the case of Ni_3Fe). The treatment of individual experimental rows was also dependent on the visible concentration of metal ions in solution (since these ions have to be removed by precipitation as hydroxides prior to NMR measurements) and is additionally described in the according figure legends. All samples were then centrifuged at 13.000 rpm for 10 min. The supernatant was then separated from the precipitate (catalyst) and stored at 4 °C overnight or longer until the NMR or HPLC analysis.

NMR analysis (for awaruite and magnetite experiments). Concentrations of formate, acetate, pyruvate and methanol (as methoxide) were determined by ^{1}H-NMR, following the protocol established in Varma et al[18]. The supernatant of the centrifuged samples was therefore mixed with sodium 3-(trimethylsilyl)-1-propanesulfonate (DSS) D_2O-solution as the internal standard

(C**H**$_3$ peak at 0 ppm). NMR spectra were acquired on a Bruker Avance III – 600 or a Bruker Avance 300 spectrometer at 297 K, using a ZGESGP pulse program. 32 scans were acquired for each sample, the relaxation delay was set to 40 s (600 MHz) and 87 s (300 MHz), with a spectral width of 12315 ppm (600 MHz) or 11963 ppm (300 MHz). Analysis and integration were performed using MestReNova (10.0.2) software. Shifts of the measured products are depicted in Extended Data Fig. 9b.

Powder X-ray diffraction (XRD). XRD analysis was performed for pre- and post-reaction catalysts. For greigite, XRD specimen was prepared as described previously[58]. In brief, the sample was collected by centrifugation, and the obtained pellet was directly mounted as a slurry form on a silicon holder (SanyuShoko), and then sealed by using polyimide film (Nilaco Corporation) and vacuum grease (JEOL) to avoid possible desiccation and oxidation during the analysis. The specimen was analysed using a RINT2000 X-ray diffractometer (Rigaku) at room temperature for CuK$\alpha_{1,2}$ radiation scanning at a step interval of 0.02° 2θ and a counting time of 2 seconds with a 2θ range from 20° to 60°, operating at an accelerating voltage of 40 kV at 30 mA. In order to prepare specimens for magnetite and awaruite experiments, the samples were collected, washed with Milli-Q water and dried under vacuum. XRD patterns of these specimens were collected at room temperature by using a theta-theta diffractometer (Stoe) in Bragg-Brentano geometry for CuK$\alpha_{1,2}$ radiation scanning at a step interval of 0.04° 2θ and a counting time of 6 seconds with a 2θ range from 20° to 80°.

Electron microscopy. Electron microscopic observation was conducted for pre-reaction catalysts to check their morphology. For greigite, a specimen for scanning electron microscopy was prepared as described previously[58]. Briefly, in the anaerobic chamber, greigite was rinsed at least three times with N_2-purged Milli-Q water, dried at room temperature, and then mounted on an aluminium stab using carbon tape. The specimen was taken out from the anaerobic chamber, coated with platinum/palladium alloy with an ion sputter E102 (Hitachi) and observed on a JSM-6330F (JEOL) or JSM-7800F (JEOL) field-emission scanning electron microscope (FE-SEM) at an acceleration voltage of 5 kV. The magnetite sample was deposited on lacey carbon film-coated Cu grids (400 mesh), and observed on an H-7100 (Hitachi) transmission electron microscope at an acceleration voltage of 100 kV. The awaruite sample was collected and embedded in Spurr resin (hard mixture). Obtained resin blocks were trimmed using an EM TRIM milling system (Leica). Thin sections were cut from the resin blocks by using a microtome with a 35° diamond knife (Reichert Ultra-Cut), dispersed in Milli-Q water and

transferred from the water surface on lacey carbon film-coated Cu grids (400 mesh), and observed on an S-5500 (Hitachi) scanning transmission electron microscope at an acceleration voltage of 30 kV.

Thermodynamic calculations. For Gibbs free energy yield (ΔG) calculations, published values of ΔH and ΔG values were used[63,64]. The effect of temperature on the Gibbs free energy yield was calculated using the Gibbs-Helmholtz equation. Equilibrium constants at different temperatures were adjusted using the van't Hoff equation (detailed equations in the Supplementary Information). Corrections based on non-standard pressures were estimated using partial molar volume changes of the reactions[65]. For any organic compounds that were not detected, an aqueous concentration of 0.1 μM was assumed. For CH_4, a partial pressure of 10^{-7} bar was assumed when not detected. In reactions containing Fe^0 as an electron donor (Supplementary Tab. 2), the H_2 concentration was estimated by assuming H_2-dependent CO_2 reduction to formate reached equilibrium. Final H_2 and CO_2 concentrations were estimated based on the measured products (subtracting 1 mol H_2 per mole formate detected).

Tables

Table 1: Changes in Gibbs free energy ΔG for the CO_2 fixation product formation in kJ mol^{-1}.

	Greigite		Magnetite		Awaruite	
Product	1	2	3	4	5	6
Formate	0.31	–25.58	–19.56	–48.14	–2.56	–15.26
Methanol	ND	ND	–46.60	–46.60	–51.49	–50.33
Acetate	–71.00	–96.69	–108.59	–137.16	–120.03	–132.17
Pyruvate	ND	ND	ND	–57.18	ND	ND

Notes:

The values of ΔG refer to the reactions as shown in equations **1**–**5**. The conditions are those of reactions marked with asterisks in Figs. 2 and 3. Details of reaction conditions for columns 1–6: 1) 0.33 mmol Fe_3S_4, 100 °C, 24 h, pH 6.5, 2 bar H_2/CO_2 (80:20); 2) 0.33 mmol Fe_3S_4, 100 °C, 24 h, pH 10, 2 bar H_2/CO_2 (80:20); 3) 0.33 mmol, Fe_3O_4, 100 °C, 16 h, pH 6, 25 bar H_2/CO_2 (40:60); 4) 0.33 mmol, Fe_3O_4, 100 °C, 16 h, pH 9, 25 bar H_2/CO_2 (40:60); 5) 0.25 mmol, Ni_3Fe, 100 °C,16 h, pH 6, 25 bar H_2/CO_2 (40:60); 6) 0.25 mmol, Ni_3Fe, 100 °C, 16 h, pH 8, 25 bar H_2/CO_2 (40:60). Columns 1, 3, 5: pH<7; Columns 2, 4, 6: pH>8. ND: not detected (no product was formed or product concentration was below the detection limit). Values of ΔG for product accumulation at 100 nM in these experiments (below the detection level) are given in Supplementary Tab. 3.

Figures

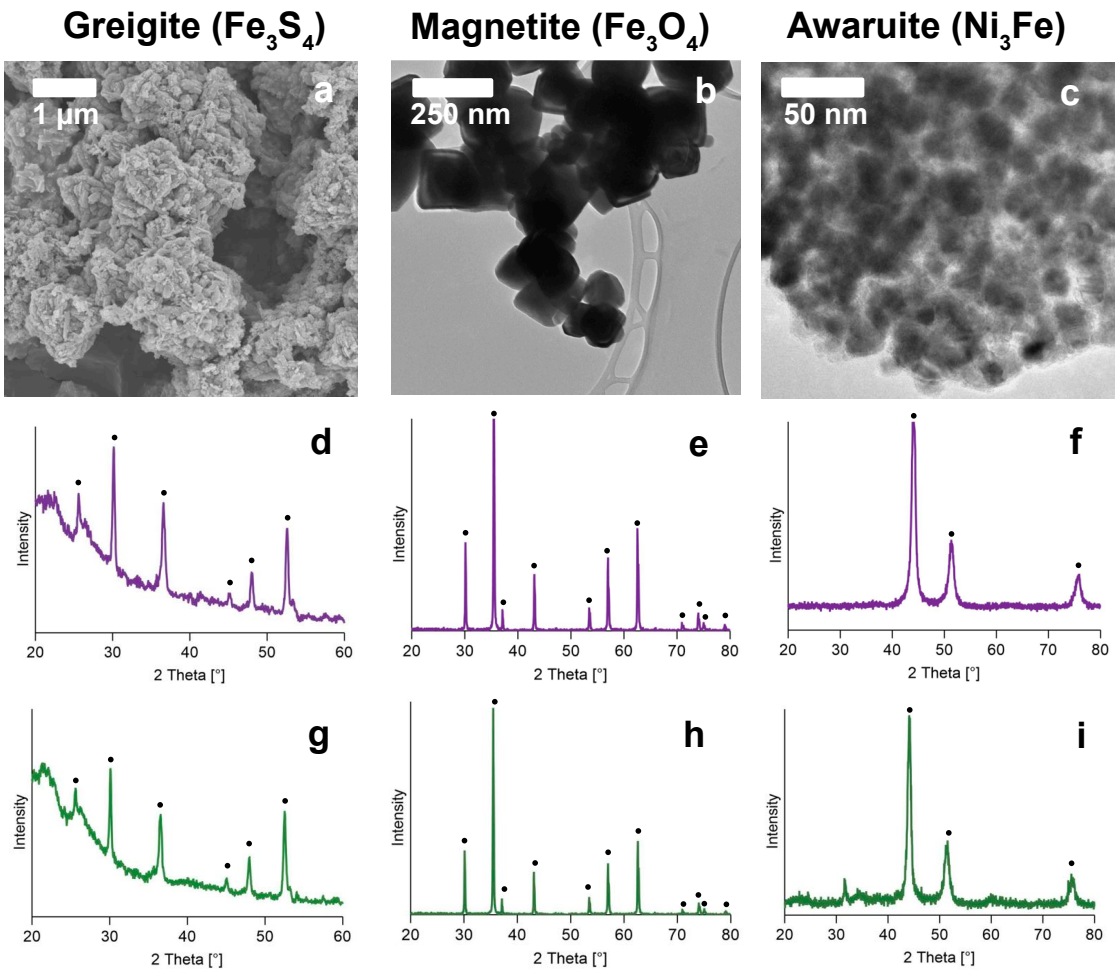

Figure 1: Characterisation of greigite (Fe_3S_4), magnetite (Fe_3O_4) and awaruite (Ni_3Fe) catalysts. The three powders are different in structure and morphology as seen from electron microscopy images (**a**, **b**, **c**), of which greigite and awaruite are freshly synthesised, magnetite is commercially obtained. Comparison of the XRD patterns of the minerals before the reaction (**d**, **e**, **f**) and after the experiments under the following conditions: Fe_3O_4 (**h**) and Ni_3Fe (**i**) for 16 h under alkaline conditions (potassium hydroxide added) under a H_2/CO_2 atmosphere. Fe_3S_4 (**g**), for 24 h at pH 6.5, stabilised by a phosphate buffer under a H_2/CO_2 atmosphere.

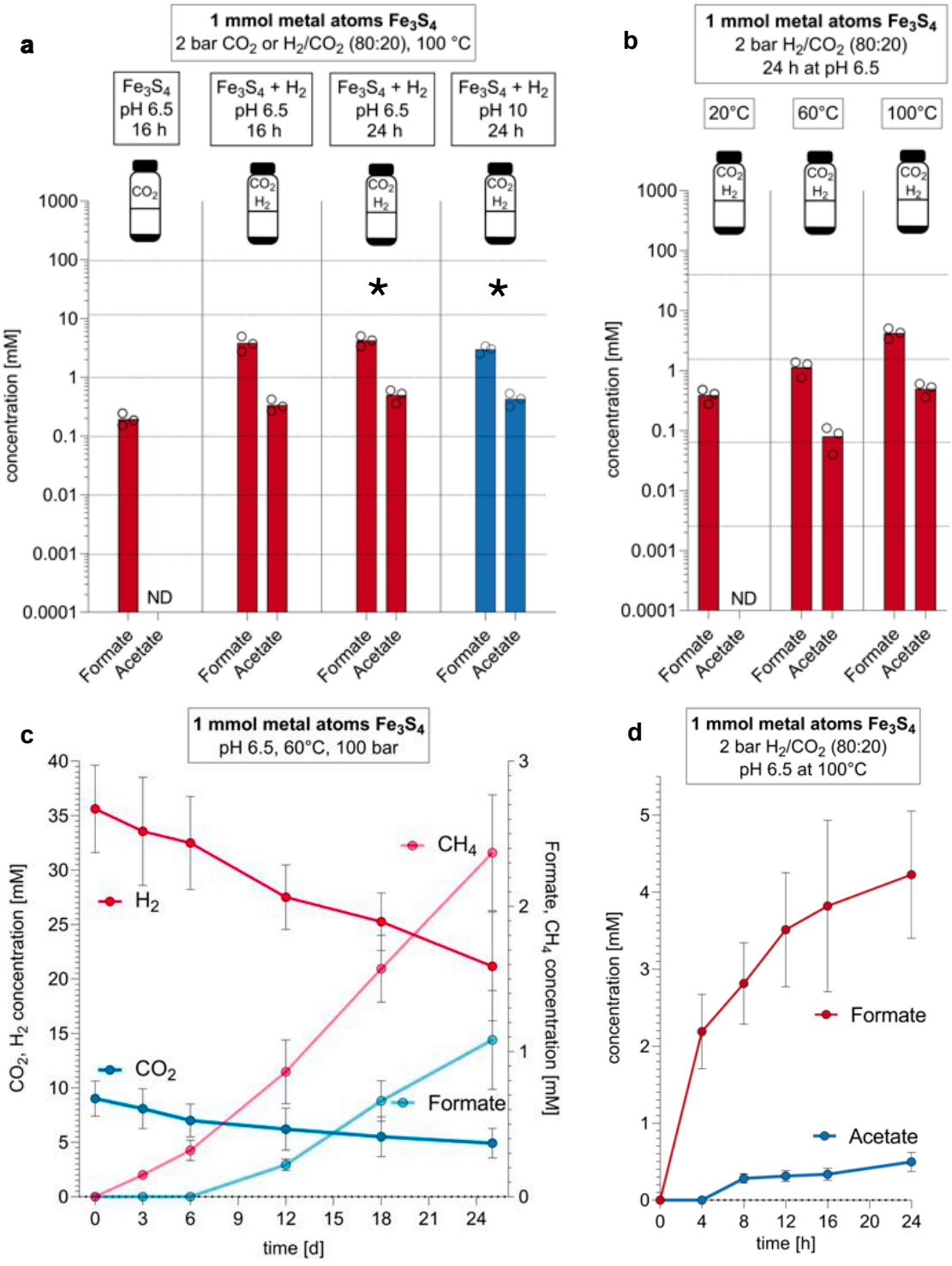

Figure 2: a Fixation of CO_2 with H_2, catalysed by greigite. **b** Effect of temperature on greigite catalysis. **c** Time course experiment of high-pressure methane and formate production from CO_2 and H_2 under greigite catalysis (liquid phase, 150 mL) at 100 bar and 60 °C. (d) Reaction progress over time at a 2 bar H_2/CO_2 atmosphere and 100 °C. All reactions were performed in water containing a phosphate buffer (3 mL for (a), (b) and (d), 150 mL for (c)). Flasks in the first two panels summarise the reaction parameters:

greigite is depicted in black. Catalyst amounts are normalised by the number of moles of metal atoms per mole of mineral compound, 0.33 mmol of greigite (Fe_3S_4) are equivalent to 1 mmol of metal atoms each. Individual experiments were performed under either CO_2 or H_2/CO_2 atmosphere. Red bars: pH<7, Blue bars: pH>7. ND: not detected (no product was formed or product concentration was below the detection limit). Circles correspond to the values of individual experiments. Values of 0 are not shown by the logarithmic scale. Asterisks indicate experiments for which the Gibbs free energy was calculated in Tab. 1. Concentration values and standard deviations of the experiments are listed in Supplementary Tab. 1, control experiments are shown in Extended Data Fig. 2a. The influence of pH (4–10) on the reactions catalysed by greigite is shown in Extended Data Fig. 4a).

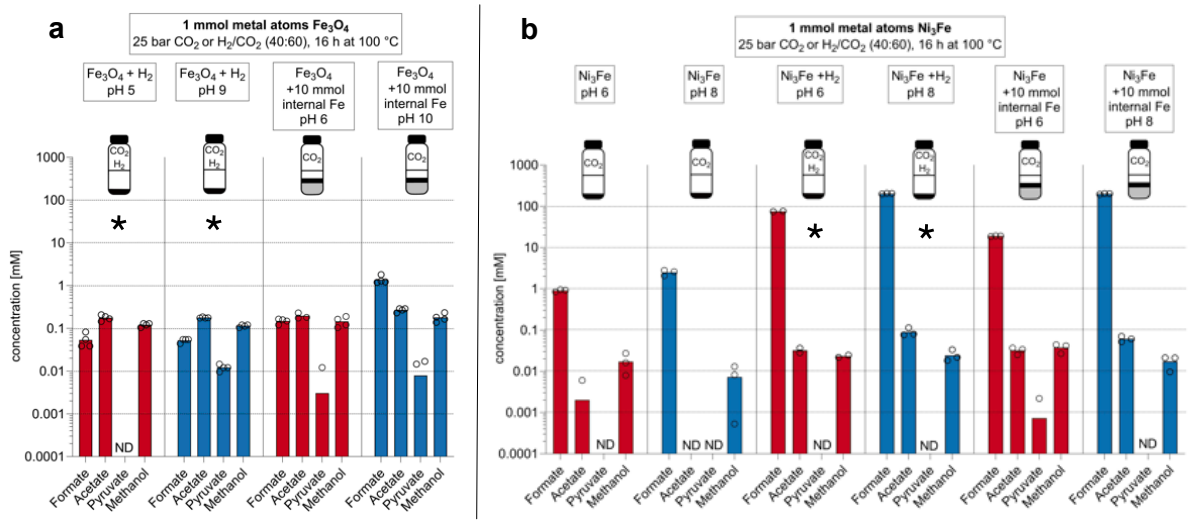

Figure 3: Fixation of CO_2 with H_2, catalysed by **a** magnetite and **b** awaruite. All reactions were performed in water (1 mL). Flasks in each panel summarise the reaction parameters: hydrothermal minerals are depicted in black, additional iron powder in grey. Catalyst amounts are normalised by the number of moles of metal atoms per mole of mineral compound: 0.33 mmol of magnetite (Fe_3O_4), as well as 0.25 mmol of awaruite are equivalent to 1 mmol of metal atoms in each catalyst. Individual experiments were performed under either CO_2 atmosphere, H_2/CO_2 atmosphere, or CO_2 atmosphere with Fe powder as an electron source (also for H_2 formation from H_2O). Experiments without native Fe were performed with decontaminated stir bars, those containing native Fe were performed without stir bars due to the solidification of the Fe powder during the process. Red bars: pH<7, Blue bars: pH>7. ND: not detected (no product was formed or product

concentration was below the detection limit). Experiments performed at pH<7 were treated with KOH after the reaction as in Varma et al.[18]. Circles correspond to the values of individual experiments. Values of 0 are not shown by the logarithmic scale. Asterisks indicate experiments for which the Gibbs free energy was calculated in Tab. 1. Concentration values and standard deviations of the experiments are listed in Supplementary Tab. 1, control experiments are shown in Extended Data Figs. 2b and c (Ni_3Fe) and 3 (Fe^0) and Supplementary Tabs. 4–7. Background levels of formate at least three orders of magnitude below experimental product concentrations (Ni_3Fe); background levels of acetate (ca. 10 to 20 µM) were observed in controls using Ni_3Fe as the catalyst. All background levels were subtracted before plotting (see Supplementary Information for all background values).

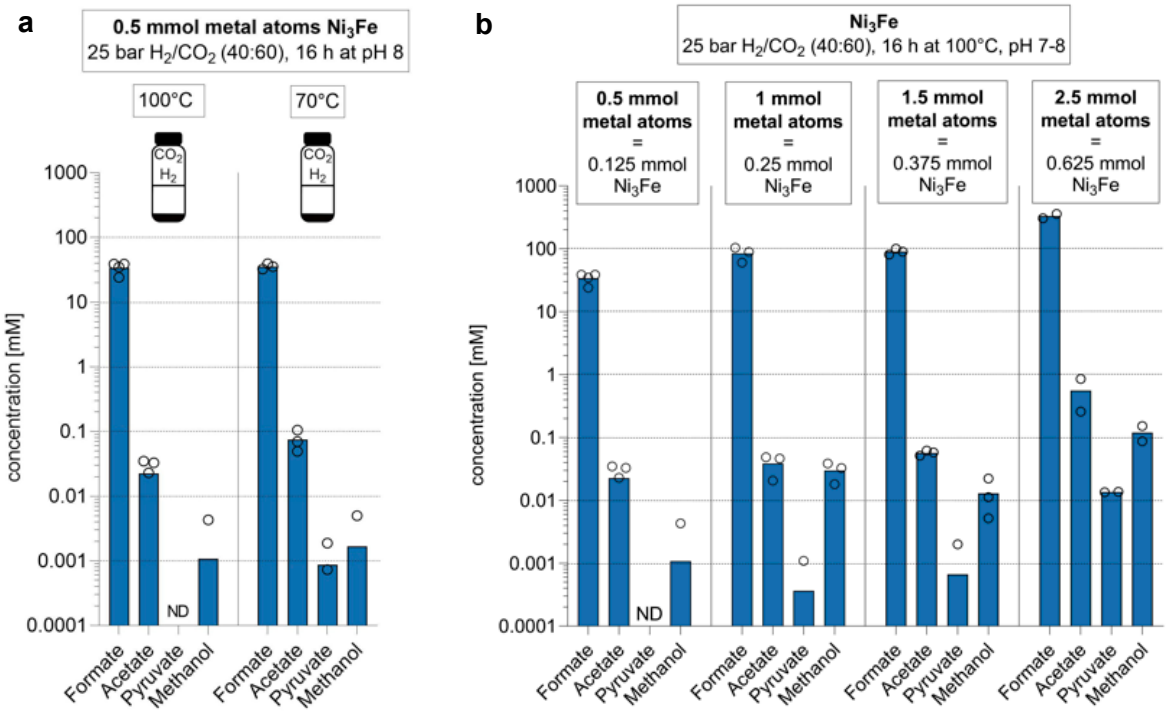

Figure 4: a Effect of temperature on Ni_3Fe catalysis. **b** Impact of Ni_3Fe catalyst amount. All reactions were performed in water (1 mL). Catalyst amounts are normalised to the number of moles of metal atoms per mole of mineral compound: 0.25 mmol of awaruite is equivalent to 1 mmol of metal atoms. Individual experiments were performed under H_2/CO_2 (40:60) atmosphere. All experiments were conducted without stir bars. Circles correspond to the values of individual experiments. Values of 0 are not shown by the logarithmic scale. All measurements were performed in at least triplicate (2.5 mmol Ni_3Fe in duplicate) ND: not detected (no product was formed or product concentration was

below the detection limit). Circles correspond to the values obtained in individual experiments. Values of 0 are not shown by the logarithmic scale. Concentration values and standard deviations of the experiments are listed in Supplementary Tab. 1, control experiments are shown in Extended Data Fig. 2b and c and Supplementary Tabs. 6 and 7.

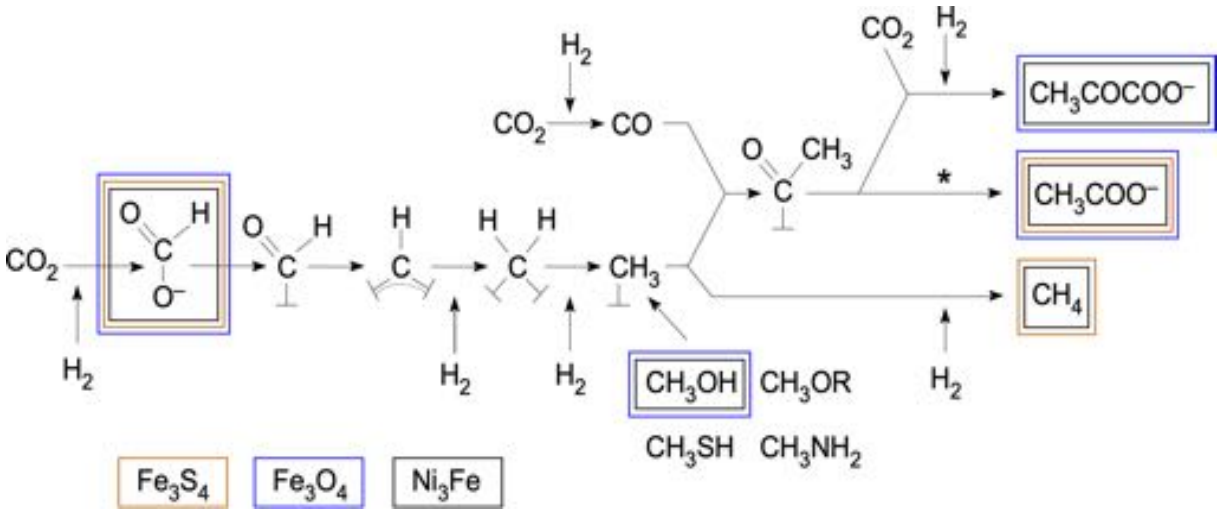

Figure 5: Congruence between the acetyl-CoA pathway and reactions catalysed by three iron minerals found in hydrothermal vents. The chemical reactions summarise the acetyl-CoA pathway as it occurs in hydrogenotrophic bacteria and archaea as depicted in ref.[11], with the exception of free formate later discovered in the archaeal pathway[66]. The methenyl (=CH–), methylene (–CH_2–), and methyl (–CH_3) groups of the bacterial and archaeal pathway are bound to tetrahydrofolate and tetrahydromethanopterin, respectively, generically indicated as catalysts (⊥) here. Coloured boxes indicate products observed in reactions using iron mineral catalysts. An asterisk indicates the reaction sequence in which energy is conserved as ATP via substrate level phosphorylation in the biological pathway (the acyl-nickel, thioester and acyl-phosphate intermediates that the enzymatic pathway employs for the stepwise conservation of free energy in the exergonic conversion of the nickel-bound acyl group to ATP[11] are not shown). All products shown were observed at temperatures ≤100 °C and obtained within <24 h, except methane in the case of greigite, which was observed over the course of 25 d (Fig. 2c). Methanol, methyl sulfide, methyl amines, and methoxy groups from coal can serve as methyl donors for the pathway[11,67].

Contributions

W.F.M. wrote the initial draft of the main text and all authors edited the manuscript. W.F.M., H.T., J.M. and M.P. designed the awaruite experiments, M.P. performed the awaruite experiments and assembled the results for the main text and SI material. K.B.M. designed and performed the magnetite experiments, S.J.V. performed exploratory experiments with magnetite. Design of the greigite experiments was done by K.I. and Y.K., K.I. performed the experiments. H.T. and M.Y. designed and synthesised the awaruite nanoparticles and performed XRD and TEM measurements for magnetite and awaruite experiments. M.K.N. performed and interpreted the thermodynamics calculations. K.K., J.M., H.T. and M.P. formulated the H_2 reduction mechanism shown in the SI.

Acknowledgements

We thank Yitao Dai for setting up gas analysis for the awaruite experiments, Andrey do Nascimento Vieira for performing parts of the revision experiments, Alexander Bähr, and Perlina Lim for scientific support and Joana C. Xavier for discussions. For funding, J.M., W.F.M. and H.T. thank the VW foundation (96_742). W.F.M. and H.T. thank the Deutsche Forschungsgemeinschaft (MA-1426/21-1 / TU 315/8-1) and W.F.M thanks the European Research Council (ERC 666053). This work is partly supported by IMPRS-RECHARGE and MAXNET Energy consortium of the Max Planck Society. K.I. and Y.K. thank JSPS KAKENHI Grant-in-Aid for Scientific Research on Innovative Areas (K.I.: JP17H05240 / Y.K.: 26106004). K.I. is also supported by Grant-in-Aid for Young Scientists B (JP17K15255). J.M. thanks the European Research Council (ERC 639170) and ANR LabEX (ANR-10-LABX-0026 CSC). This work was also partly supported by Nanotechnology Platform Program (Molecule and Material Synthesis) of the Ministry of Education, Culture, Sports, Science and Technology (MEXT), Japan.

Data Availability Statement

All data are available in the main text, Extended Data Figs. 1–10 and the Supplementary Information (Supplementary Materials and Methods, Supplementary Tables 1–7, Supplementary Figures 1–29 and Supplementary Equations).

Competing Interests

587 The authors declare no competing interests.

588

References

1. Baross, J. A. & Hoffman, S. E. Submarine hydrothermal vents and associated gradient environments as sites for the origin and evolution of life. *Orig. Life Evol. Biosph.* **15**, 327–345 (1985).
2. McCollom, T. M. Abiotic methane formation during experimental serpentinization of olivine. *Proc. Natl. Acad. Sci. U.S.A.* **113**, 13965–13970 (2016).
3. McDermott, J. M., Seewald, J. S., German, C. R. & Sylva, S. P. Pathways for abiotic organic synthesis at submarine hydrothermal fields. *Proc. Natl. Acad. Sci. U.S.A.* **112**, 7668–7672 (2015).
4. Ménez, B. *et al.* Abiotic synthesis of amino acids in the recesses of the oceanic lithosphere. *Nature* **564**, 59–63 (2018).
5. Klein, F. & Bach, W. Fe-Ni-Co-O-S phase relations in peridotite-seawater interactions. *J. Petrol.* **50**, 37–59 (2009).
6. Martin, W. F. & Russell, M. J. On the origin of biochemistry at an alkaline hydrothermal vent. *Philos. Trans. R. Soc. B Biol. Sci.* **362**, 1887–1925 (2007).
7. Preiner, M. *et al.* Serpentinization: Connecting geochemistry, ancient metabolism and industrial hydrogenation. *Life* **8**, 41 (2018).
8. Sleep, N. H., Bird, D. K. & Pope, E. C. Serpentinite and the dawn of life. *Philos. Trans. R. Soc. B Biol. Sci.* **366**, 2857–2869 (2011).
9. Schrenk, M. O., Brazelton, W. J. & Lang, S. Q. Serpentinization, carbon, and deep life. *Rev. Mineral. Geochemistry* **75**, 575–606 (2013).
10. Arndt, N. T. & Nisbet, E. G. Processes on the young Earth and the habitats of early life. *Annu. Rev. Earth Planet. Sci.* **40**, 521–549 (2012).
11. Fuchs, G. Alternative pathways of carbon dioxide fixation: Insights into the early evolution of life? *Annu. Rev. Microbiol.* **65**, 631–658 (2011).
12. Müller, V., Chowdhury, N. P. & Basen, M. Electron bifurcation: A long-hidden energy-coupling mechanism. *Annu. Rev. Microbiol.* **72**, 331–353 (2018).
13. Ragsdale, S. W. & Pierce, E. Acetogenesis and the Wood-Ljungdahl pathway of CO_2 fixation. *Biochim. Biophys. Acta* **1784**, 1873–1898 (2008).
14. Sousa, F. L. & Martin, W. F. Biochemical fossils of the ancient transition from geoenergetics to bioenergetics in prokaryotic one carbon compound metabolism. *Biochim. Biophys. Acta - Bioenerg.* **1837**, 964–981 (2014).
15. Weiss, M. C. *et al.* The physiology and habitat of the last universal common ancestor.

Nat. Microbiol. **1**, 16116 (2016).

16. Huber, C. & Wächtershäuser, G. Activated acetic acid by carbon fixation on (Fe,Ni)S under primordial conditions. *Science* **276**, 245–248 (1997).
17. He, C., Tian, G., Liu, Z. & Feng, S. A mild hydrothermal route to fix carbon dioxide to simple carboxylic acids. *Org. Lett.* **12**, 649–651 (2010).
18. Varma, S. J., Muchowska, K. B., Chatelain, P. & Moran, J. Native iron reduces CO_2 to intermediates and endproducts of the acetyl-CoA pathway. *Nat. Ecol. Evol.* **2**, 1019–1024 (2018).
19. Roldan, A. *et al.* Bio-inspired CO_2 conversion by iron sulfide catalysts under sustainable conditions. *Chem. Commun.* **51**, 7501–7504 (2015).
20. Rajendran, S. & Nasir, S. Hydrothermal altered serpentinized zone and a study of Ni-magnesioferrite–magnetite–awaruite occurrences in Wadi Hibi, Northern Oman Mountain: Discrimination through ASTER mapping. *Ore Geol. Rev.* **62**, 211–226 (2014).
21. Russell, M. J. & Hall, A. J. The emergence of life from iron monosulphide bubbles at a submarine hydrothermal redox and pH front. *J. Geol. Soc. London.* **154**, 377–402 (1997).
22. Rickard, D. & Luther, G. W. Chemistry of Iron Sulfides. *Chem. Rev.* **107**, 514–562 (2007).
23. McCollom, T. M. & Seewald, J. S. Serpentinites, hydrogen, and life. *Elements* **9**, 129–134 (2013).
24. Hunger, S. & Benning, L. G. Greigite: A true intermediate on the polysulfide pathway to pyrite. *Geochem. Trans.* **8**, (2007).
25. Findlay, A. J. *et al.* Iron and sulfide nanoparticle formation and transport in nascent hydrothermal vent plumes. *Nat. Commun.* **10**, 1597 (2019).
26. Schmitt-Kopplin, P. *et al.* High molecular diversity of extraterrestrial organic matter in Murchison meteorite revealed 40 years after its fall. *Proc. Natl. Acad. Sci. U.S.A.* **107**, 2763–2768 (2010).
27. Dayhoff, M. O. & Eck, R. V. Evolution of the structure of ferredoxin based on surviving relics of primitive amino acid sequences. *Science* **152**, 363–366 (1966).
28. White, L. M., Bhartia, R., Stucky, G. D., Kanik, I. & Russell, M. J. Mackinawite and greigite in ancient alkaline hydrothermal chimneys: Identifying potential key catalysts for emergent life. *Earth Planet. Sci. Lett.* **430**, 105–114 (2015).
29. Kelley, D. S. *et al.* An off-axis hydrothermal vent field near the Mid-Atlantic Ridge at

30° N. *Nature* (2001). doi:Doi 10.1038/35084000

30. Kelley, D. S., Baross, J. A. & Delaney, J. R. Volcanoes, Fluids, and Life at Mid-Ocean Ridge Spreading Centers. *Annu. Rev. Earth Planet. Sci.* **30**, 385–491 (2002).
31. Lang, S. Q., Butterfield, D. A., Schulte, M., Kelley, D. S. & Lilley, M. D. Elevated concentrations of formate, acetate and dissolved organic carbon found at the Lost City hydrothermal field. *Geochim. Cosmochim. Acta* **74**, 941–952 (2010).
32. Lang, S. Q. *et al.* Deeply-sourced formate fuels sulfate reducers but not methanogens at Lost City hydrothermal field. *Sci. Rep.* **8**, 755 (2018).
33. Etiope, G. & Sherwood Lollar, B. Abiotic methane on Earth. *Rev. Geophys.* **51**, 276–299 (2013).
34. Kelley, D. S. *et al.* An off-axis hydrothermal vent field near the Mid-Atlantic Ridge at 30° N. *Nature* **412**, 145–149 (2001).
35. Horita, J. & Berndt, M. E. Abiogenic methane formation and isotopic fractionation under hydrothermal conditions. *Sci. Rep.* **285**, 1055–1057 (1999).
36. Schuchmann, K. & Müller, V. Direct and reversible hydrogenation of CO_2 to formate by a bacterial carbon dioxide reductase. *Science* **342**, 1382–1385 (2013).
37. Eickenbusch, P. *et al.* Origin of short-chain organic acids in serpentinite mud volcanoes of the Mariana convergent margin. *Front. Microbiol.* **10**, 1–21 (2019).
38. Etiope, G. & Schoell, M. Abiotic gas: atypical, but not rare. *Elements* **10**, 291–296 (2014).
39. McCollom, T. M. & Seewald, J. S. Experimental constraints on the hydrothermal reactivity of organic acids and acid anions: I. Formic acid and formate. *Geochim. Cosmochim. Acta* **67**, 3625–3644 (2003).
40. McCollom, T. M. & Seewald, J. S. Carbon isotope composition of organic compounds produced by abiotic synthesis under hydrothermal conditions. *Earth Planet. Sci. Lett.* **243**, 74–84 (2006).
41. McCollom, T. M. & Seewald, J. S. A reassessment of the potential for reduction of dissolved CO_2 to hydrocarbons during serpentinization of olivine. *Geochim. Cosmochim. Acta* **65**, 3769–3778 (2001).
42. Menon, S. & Ragsdale, S. W. Unleashing hydrogenase activity in carbon monoxide dehydrogenase/acetyl-CoA synthase and pyruvate:ferredoxin oxidoreductase. *Biochemistry* **35**, 15814–15821 (1996).
43. Jeoung, J.-H. & Dobbek, H. Carbon dioxide activation at the Ni,Fe-cluster of anaerobic carbon monoxide dehydrogenase. *Conserv. Exhib.* **318**, 1461–1464 (2007).

44. Dobbek, H., Svetlitchnyi, V., Gremer, L., Huber, R. & Meyer, O. Crystal structure of a carbon monoxide dehydrogenase reveals a [Ni-4Fe-5S] cluster. *Science* **293**, 1281–1285 (2001).
45. Chabrière, E. *et al.* Crystal structures of the key anaerobic enzyme pyruvate ferredoxin oxidoreductase free and in complex with pyruvate. *Nat. Struct. Biol.* **6**, 182–190 (1999).
46. Volbeda, A. *et al.* Crystal structure of the nickel-iron hydrogenase from *Desulfovibrio gigas*. *Nature* **373**, 580–587 (1995).
47. Martin, W. F. Carbon–metal bonds: rare and primordial in metabolism. *Trends Biochem. Sci.* **44**, 807–818 (2019).
48. Buckel, W. & Thauer, R. K. Flavin-based electron bifurcation, ferredoxin, flavodoxin, and anaerobic respiration with protons (Ech) or NAD^+(Rnf) as electron acceptors: A historical review. *Front. Microbiol.* **9**, (2018).
49. Vasiliadou, R., Dimov, N., Szita, N., Jordan, S. & Lane, N. Possible mechanisms of CO_2 reduction by H_2 via prebiotic vectorial electrochemistry. *Interface Focus* (2018).
50. Kaufmann, M. On the free energy that drove primordial anabolism. *Int. J. Mol. Sci.* **10**, 1853–1871 (2009).
51. Patel, B. H., Percivalle, C., Ritson, D. J., Duffy, C. D. & Sutherland, J. D. Common origins of RNA , protein and lipid precursors in a cyanosulfidic protometabolism. *Nat. Chem.* **7**, 301–307 (2015).
52. Lane, N. & Martin, W. F. Perspective The Origin of Membrane Bioenergetics. *Cell* **151**, 1406–1416 (2012).
53. Jordan, S. F., Nee, E. & Lane, N. Isoprenoids enhance the stability of fatty acid membranes at the emergence of life potentially leading to an early lipid divide. *Interface Focus* **9**, 20100067 (2019).
54. Jordan, S. F. *et al.* Promotion of protocell self-assembly from mixed amphiphiles at the origin of life. *Nat. Ecol. Evol.* **3**, 1705–1714 (2019).
55. Kitadai, N. *et al.* Metals likely promoted protometabolism in early ocean alkaline hydrothermal systems. *Sci. Adv.* **5**, eaav7848 19 (2019).
56. Muchowska, K. B. *et al.* Metals promote sequences of the reverse Krebs cycle. *Nat. Ecol. Evol.* **1**, 1716–1721 (2017).
57. Lovley, D. R. & Phillips, E. J. Organic matter mineralization with reduction of ferric iron in anaerobic sediments. *Appl. Environ. Microbiol.* **51**, 683–689 (1986).
58. Igarashi, K., Yamamura, Y. & Kuwabara, T. Natural synthesis of bioactive greigite by

solid – gas reactions. *Geochim. Cosmochim. Acta* **191**, 47–57 (2016).

59. Kato, S., Yumoto, I. & Kamagata, Y. Isolation of acetogenic bacteria that induce biocorrosion by utilizing metallic iron as the sole electron donor. *Appl. Environ. Microbiol.* **81**, 67–73 (2015).
60. Mayumi, D. *et al.* Carbon dioxide concentration dictates alternative methanogenic pathways in oil reservoirs. *Nat. Commun.* **4**, 1–6 (2013).
61. Deng, X., Chan, C. K. & Tüysüz, H. Spent tea leaf templating of cobalt-based mixed oxide nanocrystals for water oxidation. *ACS Appl. Mater. Interfaces* **8**, 32488–32495 (2016).
62. Yu, M., Moon, G., Bill, E. & Tüysüz, H. Optimizing Ni−Fe oxide electrocatalysts for oxygen evolution reaction by using hard templating as a toolbox. *Appl. Energy Mater.* **2**, 1199–1209 (2019).
63. Hanselmann, K. W. Microbial energetics applied to waste repositories. *Experientia* **47**, 645–687 (1991).
64. Amend, J. P. & Shock, E. L. Energetics of overall metabolic reactions of thermophilic and hyperthermophilic archaea and bacteria. *FEMS Microbiol. Rev.* **25**, 175–243 (2001).
65. Wang, G., Spivack, A. J. & Hondt, S. D. Gibbs energies of reaction and microbial mutualism in anaerobic deep subseafloor sediments of ODP Site 1226. *Geochim. Cosmochim. Acta* **74**, 3938–3947 (2010).
66. Wagner, T., Ermler, U. & Shima, S. The methanogenic CO_2 reducing-and-fixing enzyme is bifunctional and contains 46 [4Fe-4S] clusters. *Science* **354**, 114–117 (2015).
67. Mayumi, D. *et al.* Methane production from coal by a single methanogen. *Science* **354**, 222–225 (2016).
68. Hoffman, B. M. *et al.* Mechanism of nitrogen fixation by nitrogenase: the next stage. *Chem. Rev.* **114**, 4041–62 (2014).